CHEMISTRY OF MATERIALS
Communication

Chem. Mater. **2010,** *22,* 6215–6217 6215
DOI:10.1021/cm102414n

In situ Supported Nanoscale $Ru_xTi_{1-x}O_2$ on Anatase TiO_2 with Improved Electroactivity

Ruiyong Chen,[†] Vinh Trieu,[†] Harald Natter,[†] Klaus Stöwe,[‡] Wilhelm F. Maier,[‡] Rolf Hempelmann,*[,†] Andreas Bulan,[§] Jürgen Kintrup,[§] and Rainer Weber[§]

[†]*Physikalische Chemie, and* [‡]*Technische Chemie, Universität des Saarlandes, 66123 Saarbrücken, Germany, and* [§]*Bayer MaterialScience AG, 51368 Leverkusen, Germany*

Received August 22, 2010
Revised Manuscript Received November 2, 2010

RuO_2−TiO_2 has been used as benchmark anode catalysts over the past four decades in the energy-intensive chlor-alkali process,[1] which is one of the largest industrial technological applications of electrocatalysis. It is critically needed to boost the energy efficiency in industrial processes by using electrocatalysts with improved activity. Employed as electrode materials, RuO_2-based oxide coatings on a metal substrate are routinely prepared by oxidative pyrolysis[2] or sol−gel techniques.[3] The growth and aggregation of active particles is accompanied by the combustion of organics during thermal treatment, which is used to obtain higher crystallinity and mechanical stability for practical applications.[4] Nanoscale control in particle size (a few nanometers) and dispersion is promising in optimizing the properties of the catalysts.[5] Atomic scale surface analysis[6] and density functional theory calculations[7] of the RuO_2 revealed that the coordinatively unsaturated sites (cus) of ruthenium and bridging oxygen atoms determine the catalytic reactivity. Stabilizing the nanophase against growth and aggregation becomes one of the most important concerns and challenges in the design of materials to explore the size-dependent properties.

So far, the advances in fabrication of oxide nanomaterials are primarily based on the colloid chemistry route due to its low-cost and versatile character, wherein the crystal growth or aggregation of nanoparticles can be retarded by using surface ligands or stabilizers.[8] However, the decomposition of organic ligands is often strongly temperature dependent, thus a conflict exists between the optimized thermal treatment conditions to achieve functions described above and simultaneous preservation of the character of the pristine particles. Besides, the embedded impurities in the final products may be unfavorable for catalytic applications.[9] It is highly desirable to develop innovative, ligand-independent routes to fabricate high-temperature stable nanoscale oxide materials.

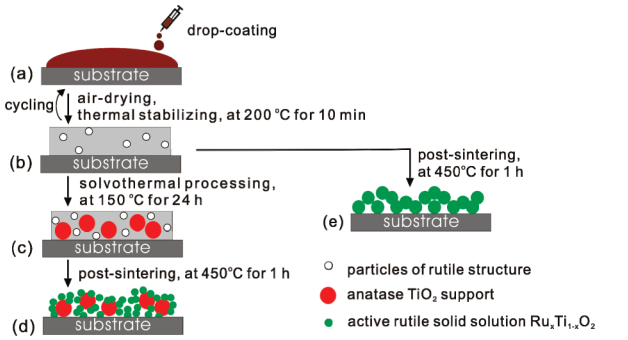

Figure 1. Schematic illustration of the coating structure formation of in situ supported rutile nanocrystals $Ru_xTi_{1-x}O_2$ onto anatase TiO_2 with the route (a→b→c→d): (a) wet coating applied to the substrate; (b) Ru−O−Ti xerogel coating with rutile-type local order structure; (c) coating containing anatase TiO_2 precrystallized by solvothermal processing of (b); and (d) coating with supported structure of $Ru_xTi_{1-x}O_2/TiO_2$ after postsintering treatment of (c). For comparison, coating was prepared via the conventional route (a→b→e).

Herein, we report a facile preparation strategy to obtain a novel coating structure with in situ supported active nanoscale $Ru_xTi_{1-x}O_2$ (3 nm) on inert anatase TiO_2 (20 nm) by using a combined sol−gel/solvothermal route (see the Supporting Information). As illustrated in Figure 1, the controlled preparation is starting from the amorphous Ru−O−Ti xerogel coatings containing nanoparticles of rutile structure (Figure 1b). The anatase TiO_2 supports are obtained in situ by solvothermal crystallization of the amorphous xerogel coating. Subsequent sintering treatment results in crystallization of the solid solution of active rutile $Ru_xTi_{1-x}O_2$ nanocrystals, the grain growth of which is inhibited because of the isolation effects of the precrystallized anatase TiO_2 support particles. The coatings with this unique supported structure of $Ru_xTi_{1-x}O_2/TiO_2$ have been proven to be highly active for the electrochemical evolution of chlorine (EEC), compared to the coatings prepared via the conventional route and a commercial $Ru_{0.3}Ti_{0.7}O_2$ coating.

*Corresponding author. E-mail: r.hempelmann@mx.uni-saarland.de.

(1) (a) Beer, H. B. British Patent 1 147 442, 1965. (b) De Nora, O. *Chem. Eng. Technol.* **1970**, *42*, 222. (c) Trasatti, S. *Electrochim. Acta* **2000**, *45*, 2377. (d) Moussallem, I.; Jörissen, J.; Kunz, U.; Pinnow, S.; Turek., T. *J. Appl. Electrochem.* **2008**, *38*, 1177.
(2) (a) Hine, F.; Yasuda, M.; Yoshida, T. *J. Electrochem. Soc.* **1977**, *124*, 500. (b) Arikawa, T.; Takasu, Y.; Murakami, Y.; Asakura, K.; Iwasawa, Y. *J. Phys. Chem. B* **1998**, *102*, 3736.
(3) Panić, V. V.; Dekanski, A.; Milonjić, S. K.; Atanasoski, R. T.; Nikolić, B. Ž. *Colloids Surf., A* **1999**, *157*, 269.
(4) Roginskaya, Yu. E.; Morozova, O. V. *Electrochim. Acta* **1995**, *40*, 817.
(5) Schlögl, R.; Abd Hamid, S. B. *Angew. Chem., Int. Ed.* **2004**, *43*, 1628.
(6) Over, H.; Kim, Y. D.; Seitsonen, A. P.; Wendt, S.; Lundgren, E.; Schmid, M.; Varga, P.; Morgante, A.; Ertl, G. *Science* **2000**, *287*, 1474.
(7) Hansen, H. A.; Man, I. C.; Studt, F.; Abild-Pedersen, F.; Bligaard, T.; Rossmeisl, J. *Phys. Chem. Chem. Phys.* **2010**, *12*, 283.
(8) (a) Wu, N. L.; Wang, S. Y.; Rusakova, I. A. *Science* **1999**, *285*, 1375. (b) Chen, B.; Zhang, H.; Gilbert, B.; Banfield, J. F. *Phys. Rev. Lett.* **2007**, *98*, 106103.
(9) (a) Joo, S. H.; Park, J. Y.; Tsung, C. K.; Yamada, Y.; Yang, P.; Somorjai, G. A. *Nat. Mater.* **2009**, *8*, 126. (b) Gupta, G.; Stowell, C. A.; Patel, M. N.; Gao, X.; Yacaman, M. J.; Korgel, B. A.; Johnston, K. P. *Chem. Mater.* **2006**, *18*, 6239. (c) Feng, Y.; He, T.; Alonso-Vante, N. *Chem. Mater.* **2008**, *20*, 26.

Published on Web 11/17/2010

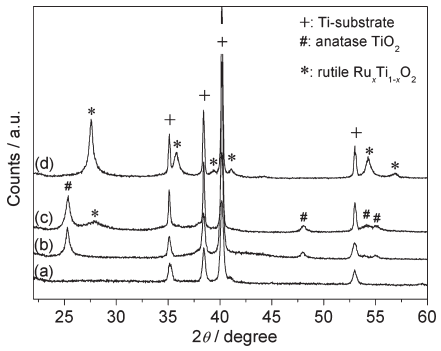

Figure 2. XRD patterns of electrodes with coatings a−d corresponding to b−e in Figure 1. (#) anatase TiO_2 (JCPDS 78−2486), (*) rutile (JCPDS 40−1290 (RuO_2), 21−1276 (TiO_2)), (+) Ti -substrate (JCPDS 44−1294).

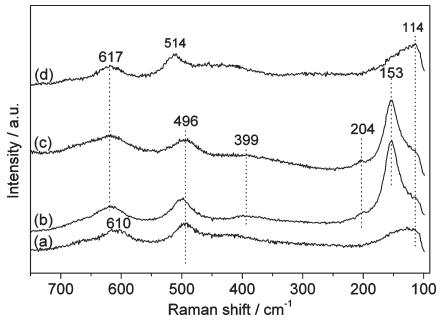

Figure 3. Raman spectra of electrodes with coatings a−d corresponding to b−e in Figure 1.

For the sol−gel derived mixed oxide materials, the M−O−M′ bonds are formed in the early stage of sol formation via the condensation reactions among the hydroxyl groups. After the deposition of the sols onto the Ti-substrate followed by partial removal of the solvents, the Ru−O−Ti xerogel networks are formed. X-ray diffraction (XRD) shows the initial Ru−O−Ti xerogel coatings were amorphous, and only the diffraction peaks of the Ti-substrate were observed (Figure 2a). Raman spectra, applied as a sensitive local probe, show the vibration bands at 610 and 114 cm^{-1}, assigned to the A_{1g} and B_{1u} mode of the rutile lattice (Figure 3a),[10] suggesting the formation of rutile particles within the xerogel coatings (Figure 1b). Further phase transformations of the deposited Ru−O−Ti xerogel coatings on Ti-substrate with and without solvothermal processing were studied by XRD and Raman spectroscopy.

Only anatase formation was detected after the solvothermal (SVT) crystallization of the amorphous Ru−O−Ti xerogels at 150 °C for 24 h (SVT coating, Figure 2b). Consistent with the XRD results, a new sharp Raman band at 153 cm^{-1} along with weak bands at 204, 399 cm^{-1} can be assigned to the anatase characteristic bands of $E_{g(1)}$, $E_{g(2)}$, B_{1g}, respectively[11] (Figure 3b). A rutile phase with a weak and broad (110) peak appears after the postsintering (PST) of the SVT coatings (SVT-PST coating, Figure 2c). The crystal growth of the rutile structure in the SVT-PST coating is retarded significantly (3 nm) (Table 1). The rutile phase detected in SVT-PST coating probably originates from growth of the initial rutile nanoparticles within the xerogel coatings on the local scale surrounding the anatase phase (20 nm) (Table 1). In contrast, rutile with a crystallite size of 17 nm was formed exclusively by direct thermal sintering of the Ru−O−Ti xerogel coatings at 450 °C for 1 h (PST coating, Figure 2d).

The lattice parameters obtained by Rietveld refinement (as summarized in Table 1) confirmed the formation of rutile $Ru_xTi_{1-x}O_2$ solid solution in the SVT-PST coating, where $x = 0.7$ was calculated using Vegard's rule.[12] The Raman bands at 496 cm^{-1} (Figure 3a-c) show the evident shift from the E_g mode positions of rutile TiO_2 nanocrystals (447 cm^{-1})[13] and rutile RuO_2 nanocrystals (511 cm^{-1}),[14] which is caused by the lattice distortion arising from the incorporation of Ti into the RuO_2. There is no evidence for Ru incorporation into the anatase TiO_2 lattice for the SVT-PST coating. These results reveal that the SVT-PST coating consists of rutile-type $Ru_{0.7}Ti_{0.3}O_2$ solid solution and undoped anatase TiO_2. Along with the quantitative Rietveld phase analysis (Table 1), the calculated Ru:Ti molar ratio in the SVT-PST coating is 41:59, which agrees well with the nominal composition (40:60). However, for the PST coating, the existence of a ruthenium-containing amorphous structure in the oxide matrix was confirmed by the Raman band at 514 cm^{-1} (Figure 3d) attributed to RuO_2 E_g mode,[14] since no separated RuO_2 phase has been detected in the XRD. Prior studies showed the complete crystallization of the Ru−O−Ti xerogel at higher temperatures (> 500 °C).[15] It can be concluded that solvothermal processing effectively assists crystallization.

Unlike the O_2-rich thermal sintering, the solvothermal processing creates a particular crystallization environment, wherein atomic short-range diffusion, organics removal, and restricted grain growth occur within the xerogel networks at mild temperature under elevated pressure conditions.[16] Transmission electron microscopy (TEM) images of the powders scratched from the SVT-PST coatings (see Figure S2 in the Supporting Information) show the 20 nm sized, well-crystallized anatase TiO_2 particles, and the neighboring rutile $Ru_xTi_{1-x}O_2$ domains of a few nanometers in size with orientational disorder and lattice distortions. The phase stabilization of the nanostructural TiO_2 exhibits a strong dependence on particle size and surface chemistry.[17] The as-obtained anatase TiO_2 particles are thermally stable during the

(10) (a) Swamy, V. *Phys. Rev. B* **2008**, *77*, 195414. (b) Ocaña, M.; Fornés, V.; García Ramos, J. V.; Serna, C. J. *J. Solid State Chem.* **1988**, *75*, 364.
(11) (a) Liu, H.; Yang, W.; Ma, Y.; Cao, Y.; Yao, J.; Zhang, J.; Hu, T. *Langmuir* **2003**, *19*, 3001. (b) Oliveira, M. M.; Schnitzler, D. C.; Zarbin, A. J. G. *Chem. Mater.* **2003**, *15*, 1903.
(12) Vegard, L. *Z. Phys.* **1921**, *5*, 17.
(13) Nakano, H.; Hasuike, N.; Kisoda, K.; Nishio, K.; Isshiki, T.; Harima, H. *J. Phys.: Condens. Matter* **2009**, *21*, 064214.
(14) (a) Korotcov, A. V.; Huang, Y. S.; Tiong, K. K.; Tsai, D. S. *J. Raman Spectrosc.* **2007**, *38*, 737. (b) Chang, K. H.; Hu, C. C.; Chou, C. Y. *Chem. Mater.* **2007**, *19*, 2112.
(15) Colomer, M. T.; Velasco, M. J. *J. Eur. Ceram. Soc.* **2007**, *27*, 2369.
(16) Cushing, B. L.; Kolesnichenko, V. L.; O'Connor, C. J. *Chem. Rev.* **2004**, *104*, 3893.
(17) (a) Li, G.; Li, L.; Boerio-Goates, J.; Woodfield, B. F. *J. Am. Chem. Soc.* **2005**, *127*, 8659. (b) Barnard, A. S.; Curtiss, L. A. *Nano Lett.* **2005**, *5*, 1261.

Table 1. Results of Rietveld Refinement of XRD Data

coating	phase	space group	phase wt %	a (Å)	c (Å)	crystallite size[a] (nm)
SVT-PST	rutile	$P4_2/mnm$	66.3	4.526(4)	3.066(5)	3.4(2)
	anatase	$I4_1/amd$	33.7	3.788(1)	9.497(4)	20.3(7)
PST	rutile	$P4_2/mnm$	100	4.575(1)	2.997(1)	17.2(4)

[a] The crystallite sizes are quoted in terms of volume averaged column heights.

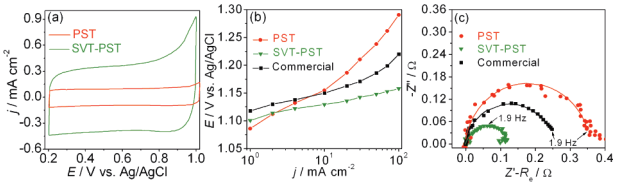

Figure 4. (a) Cyclovoltammograms recorded with a scan rate of 20 mV s^{-1} at room temperature. (b) Polarization curves recorded at 50 °C. (c) Nyquist plots measured under galvanostatic mode (56.6 mA cm^{-2}), real part is corrected by removing the electrolyte ohmic resistance (R_e). Electrolyte: 3.5 M NaCl, pH 3. Commercial $Ru_{0.3}Ti_{0.7}O_2$ coating with a Ru metal loading of 12.1 g m^{-2}.

postsintering treatment and thus act as an ideal support for the subsequent dispersion of the active rutile phase.[18] Because of the steric barrier effects of support and the restrained thermal motion of rutile particles, the growth of rutile particle during the postsintering is inhibited, which is beneficial for the practical applications. Although the undoped anatase TiO_2 is insulating, the electronic conduction path could be assured by interconnected particles of rutile $Ru_{0.7}Ti_{0.3}O_2$ or rutile particles separated with very small gaps (tunneling effect).[19]

The capacitive behavior of the obtained oxide coatings was examined by cyclic voltammetry in acidified NaCl electrolyte (Figure 4a). The number of electrochemically active sites of the coatings,[20] estimated in terms of the integrated area of the anodic branches in the cyclovoltammograms, shows a 4-fold increase in the SVT-PST coating compared to those in the PST coating with larger crystal dimension. This is roughly close to the increase in geometric surface area calculated by decreasing the crystal size from 17 to 3 nm, assuming spherical particle morphology. This suggests that active rutile nanocrystals in the SVT-PST coating are highly dispersed and electrochemically accessible.

To examine the catalytic performance for the EEC, galvanostatic polarization measurements were performed for the SVT-PST, PST and a commercial $Ru_{0.3}Ti_{0.7}O_2$ coating (Figure 4b). The SVT-PST coating (10.3 g of Ru m^{-2}) is extraordinarily more active, it can catalyze the EEC reactions at a significantly reduced electrode potential of 1.16 V at the applied current density of 100 mA cm^{-2}, corresponding to a decrease of 120 and 60 mV in comparison with the PST coating and the commercial coating, respectively. Electrochemical impedance spectroscopy was employed to further investigate the activity of the electrode coatings (Figure 4c). The semicircles can be attributed to the EEC reactions at the interface between the catalytic coating and the electrolyte.[21] The charge-transfer resistance for the SVT-PST, PST, and commercial coating are 0.12, 0.36, and 0.25 Ω, respectively, which indicates the better activity of the SVT-PST coating. The SVT-PST coating is electrochemically stable under our experimental conditions. Several aspects could be responsible for the enhancement in electrocatalytic activity of the in situ supported rutile nanocrystals: (i) the increased fraction of cus sites due to the reduced particle dimension;[6] (ii) the complete crystallization and organic impurities-free catalyst surface assured by the solvothermal processing;[16] (iii) the possible epitaxy-induced lattice strain[22] of rutile nanophase sitting on the anatase TiO_2 support particles. The investigation of the effect of support materials on the catalytic reactions is in progress in our laboratory.

In summary, a novel structure of electrocatalytic coating with in situ supported active nanocrystals $Ru_{0.7}Ti_{0.3}O_2$ onto anatase TiO_2 has been presented. Solvothermal crystallization plays a critical role in the formation of anatase particles, which stabilize the high dispersion and inhibit the growth and agglomeration of active rutile particles. This structural and crystal size-controlled preparation strategy of mixed oxide catalyst coatings can be broadly applied to the design of multicomponent heterocatalysts and has promise as electrocatalyst fabrication route for current industrial applications.

Acknowledgment. The authors gratefully acknowledge financial support from the BMBF (FKZ: 033R018G).

Supporting Information Available: Experimental part, Rietveld refinement results for PST and SVT-PST coatings, TEM for the powders scratched from the SVT-PST coatings. This material is available free of charge via the Internet at http://pubs.acs.org.

(18) Pillai, S. C.; Periyat, P.; George, R.; McCormack, D. E.; Seery, M. K.; Hayden, H.; Colreavy, J.; Corr, D.; Hinder, S. J. *J. Phys. Chem. C* **2007**, *111*, 1605.
(19) Ryan, J. V.; Berry, A. D.; Anderson, M. L.; Long, J. W.; Stroud, R. M.; Cepak, V. M.; Browning, V. M.; Rolison, D. R.; Merzbacher, C. I. *Nature* **2000**, *406*, 169.
(20) Galizzioli, D.; Tantardini, F.; Trasatti, S. *J. Appl. Electrochem.* **1974**, *4*, 57.
(21) (a) Burrows, I. R.; Denton, D. A.; Harrison, J. A. *Electrochim. Acta* **1978**, *23*, 493. (b) Alves, V. A.; Da Silva, L. A.; Boodts, J. F. C. *J. Appl. Electrochem.* **1998**, *28*, 899.
(22) (a) Jirkovský, J.; Makarova, M.; Krtil, P. *J. Electrochem. Soc.* **2005**, *152*, A1613. (b) Ruban, A.; Hammer, B.; Stoltze, P.; Skriver, H. L.; Norskov, J. K. *J. Mol. Catal. A* **1997**, *115*, 421.